

# Impacts of the Morphology of New Neighborhoods on Microclimate and Building Energy Use<sup>☆</sup>

Melissa R. Allen-Dumas<sup>a,\*</sup>, Amy N. Rose<sup>c</sup>, Joshua R. New<sup>b</sup>, Olufemi A. Omitaomu<sup>a</sup>, Jiangye Yuan<sup>a</sup>, Marcia L. Branstetter<sup>a</sup>, Linda M. Sylvester<sup>a</sup>, Matthew B. Seals<sup>c</sup>, Thomaz M. Carvalhaes<sup>a</sup>, Mark B. Adams<sup>b</sup>, Mahabir S. Bhandari<sup>b</sup>, Som S. Shrestha<sup>b</sup>, Jibonananda Sanyal<sup>a</sup>, Anne S. Berres<sup>a</sup>, Carl P. Kolosna<sup>a</sup>, Katherine S. Fu<sup>a</sup>, Alexandra C. Kahl<sup>a</sup>

<sup>a</sup>*Computational Science and Engineering Division, Oak Ridge National Laboratory, One Bethel Valley Road, Oak Ridge, TN 37831*

<sup>b</sup>*Energy and Transportation Science Division, Oak Ridge National Laboratory, One Bethel Valley Road, Oak Ridge, TN 37831*

<sup>c</sup>*National Security Emerging Technologies Division, Oak Ridge National Laboratory, One Bethel Valley Road, Oak Ridge, TN 37831*

---

## Abstract

In anticipation of emerging global urbanization and consequent increases in energy use and carbon dioxide emissions, better understanding and quantification of climate effects on energy use in cities are needed, requiring coordinated research into large-scale, regional, and microclimate impacts to and from the city structure. The methodology described here addresses this need by (1) demonstrating a process for creating and testing example morphologies for new neighborhoods for their impact on local and regional meteorology within a

---

<sup>☆</sup>This manuscript has been authored by UT-Battelle LLC under contract DE-AC05-00OR22725 with the US Department of Energy (DOE). The US government retains and the publisher, by accepting the article for publication, acknowledges that the US government retains a nonexclusive, paid-up, irrevocable worldwide license to publish or reproduce the published form of this manuscript, or allow others to do so, for US government purposes. DOE will provide public access to these results of federally sponsored research in accordance with the DOE Public Access Plan (<http://energy.gov/downloads/doe-public-access-plan>).

\*Corresponding author

*Email addresses:* [allenm@ornl.gov](mailto:allenm@ornl.gov) (Melissa R. Allen-Dumas), [rosean@ornl.gov](mailto:rosean@ornl.gov) (Amy N. Rose), [newjr@ornl.gov](mailto:newjr@ornl.gov) (Joshua R. New), [omitaomua@ornl.gov](mailto:omitaomua@ornl.gov) (Olufemi A. Omitaomu), [jiangye07@gmail.com](mailto:jiangye07@gmail.com) (Jiangye Yuan), [branstetterm@ornl.gov](mailto:branstetterm@ornl.gov) (Marcia L. Branstetter), [lsylvest@gmail.com](mailto:lsylvest@gmail.com) (Linda M. Sylvester), [sealsmb@ornl.gov](mailto:sealsmb@ornl.gov) (Matthew B. Seals), [tcarval3@asu.edu](mailto:tcarval3@asu.edu) (Thomaz M. Carvalhaes), [adamsmb@ornl.gov](mailto:adamsmb@ornl.gov) (Mark B. Adams), [bhandarims@ornl.gov](mailto:bhandarims@ornl.gov) (Mahabir S. Bhandari), [shresthass@ornl.gov](mailto:shresthass@ornl.gov) (Som S. Shrestha), [sanyalj@ornl.gov](mailto:sanyalj@ornl.gov) (Jibonananda Sanyal), [berresas@ornl.gov](mailto:berresas@ornl.gov) (Anne S. Berres), [ckolosna@gmail.com](mailto:ckolosna@gmail.com) (Carl P. Kolosna), [fu.katherine@gmail.com](mailto:fu.katherine@gmail.com) (Katherine S. Fu), [kahlac@ornl.gov](mailto:kahlac@ornl.gov) (Alexandra C. Kahl)

two-way-coupled four-domain nested mesoscale weather model (6 km horizontal resolution outer domain, 90 m horizontal innermost domain) and (2) allocating resulting building-level meteorological profiles to each building in a neighborhood for parallel computation of building-by-building energy use. Our Chicago Loop test case shows that the morphology of even a small new added development to a neighborhood affects not only its own microclimate, but also the microclimate of the original neighborhood to which the development was added, and that these changes in microclimate affect both neighborhoods' building energy use. This method represents an important step toward quantifying and analyzing the relationships among climatic conditions, urban morphology, and energy use and using these relationships to inform energy-efficient urban development and planning.

*Keywords:* urban morphology, microclimate, building energy use, carbon dioxide emissions

---

## 1. Introduction and Background

Global and regional climates are primary drivers of heating and cooling demand for buildings. The United States, comprising only 4.4% of the world's population, consumes 19% of the world's primary energy production. In 2010, buildings accounted for the largest fraction (41%) of primary energy consumption. This fraction of consumption amounts to 40% of total US carbon dioxide ( $CO_2$ ) emissions, contributing significantly to global warming and to regional climate change [1]. Climate change impacts, urban and rural population growth, and concomitant increases in energy demands have the potential to alter regional energy consumption patterns as more humans respond to new climate conditions. The added consumption may then result in even higher quantities of emissions that accelerate ecological change [2].

Yet the responses of specific buildings to atmospheric conditions are not to synoptic or even mesoscale weather, but to the local-scale conditions, as modified by the structure of the neighborhood in which the buildings stand [3].

This urban microclimate, determined by local meteorology, solar irradiation and reflection, and surface temperatures of buildings and ground, can strongly affect building energy demand. That is, buildings within an urban setting must generally respond to higher ambient temperatures due to radiation exchange  
20 between neighboring buildings, convective heat transfer due to wind patterns within a configuration, the thermal mass of city infrastructure, and other urban heat island effects [4]. This situation can offset heating demand during colder months, but it may lead to higher demand for cooling in the summer [5]. Thus, urban form may enhance or mitigate large-scale weather effects on buildings  
25 and building energy use, and changes in heretofore typical weather patterns may cause unforeseen responses from urban neighborhoods. As these weather patterns change with predicted overall warming trends, methods are needed that connect microclimate and regional climate to the global climate and that incorporate local impacts and feedbacks.

30 The uncertainty related to future climate and its effect on urban areas makes energy-efficient planning difficult, especially if no modeling frameworks include these feedbacks from the building level to the large-scale meteorology [6]. As of the Intergovernmental Panel on Climate Change Fifth Assessment Report, modeling of human impacts to climate change involved running integrated assess-  
35 ment models to obtain concentrations of greenhouse gases and the locations and extent of land use changes that will lead to different radiative forcing amounts by the end of the century [7]. To begin to facilitate two-way coupling of these models at the global scale, Collins et al. [8] coupled an integrated assessment model with an Earth system model. However, methods for connecting these  
40 global results to local action remained uninvestigated.

One step toward understanding the impact of cities on the global climate was taken by Creutzig et al. [9], who examined 274 cities of all sizes and regions worldwide and showed that economic activity, transport costs, geographic factors, and urban form explain 37% of urban direct energy use and 88% of urban  
45 transport energy use. They noted that if current trends in urban expansion continue, urban energy use by 2050 could increase to at least three times the

amount used in 2005. But sound urban planning and transport policies may be able to limit this massive increase in urban energy use and allow cities to have a large mitigating impact. However, cities are not homogeneous, and effective policies for increasing energy efficiency and reducing urban greenhouse gas emissions are likely to differ with city type. For example, while the percentage of  $CO_2$  emissions by end use sector in 2012 for the United States as a whole was 18.1% for industry, 35.3% for transportation, and 46.6% for buildings [10], individual cities do not exactly follow these trends. The greatest share of Chicago's  $CO_2$  emissions (2010) was from buildings at 71% [11]. In Los Angeles (2014), a much larger share of emissions is attributed to industry, at 25%, with buildings contributing only 40%. [12].

Building energy consumption and resulting environmental pollution owes much to a city's morphology, and a city's future sustainability can be enhanced by strategic design [13]. For example, at neighborhood scale (500 m x 500 m), it has been shown [14] that residential building type, density (ratio of building footprint area to grid cell area), building height, surface-to-volume ratio, and open space ratio (ratio of undeveloped area to grid cell area) in cities (i.e., urban morphology) all significantly impact heat-energy demand for northern latitude (41–53N) European cities. For example, differences in five idealized neighborhood morphologies (e.g., compact urban block, detached housing, high-rise apartments, and slab housing) in the four cities of London, Paris, Berlin, and Istanbul showed per-city heat-energy use savings from 11% to 73% from the least to the most efficient urban form. Differences in building density (defined as the sum of the areas of all building floors to the sample block area) among these locations accounted for 54% to 83% energy savings per city. It was also determined that among these cities, heat-energy demand decreased logarithmically with an increase in average building height and that lower surface-to-volume ratios for buildings amounted to less overall heat-energy use. However, the study did not investigate the effects of morphology on cooling-energy demand, nor did it model detailed micrometeorology within the actual urban terrain of these cities, validate findings with real data, or produce projections of energy

use based on climate or city development. Taha et al. [15] did examine the effects of changes in albedo of urban surfaces at 500 m horizontal resolution  
80 using measurements in the Los Angeles area, and showed resulting changes in the location and intensity of Los Angeles urban heat islands. But they did not try to incorporate these results into a physical model of the area.

Other researchers have examined the impacts of climate change on energy consumption and the effect of consequent urban microclimate on building energy  
85 performance [16]. For example, [17] used a building-energy model to develop a hypothetical community of statistically representative building types and to generate hourly building energy demand for these communities; but the study showed limited evaluation of microclimate effects regarding building proximity, height, and actual representative 3D configuration of cities (morphology).  
90 Progress in this area has been limited by the lack of available meteorological measurements at the resolutions needed (meteorological inputs into building energy models of neighborhoods are traditionally informed by long-term measurements at the single closest meteorological station rather than by ambient conditions around each building [18]) and by lack of access to 3D data sets for  
95 urban land surface at neighborhood scales.

To begin to look at higher-resolution processes in neighborhoods such as convective heat transfer among buildings, computational fluid dynamics experiments have been performed [e.g., 19], coupling these models to building energy simulations. However, because of the computational intensity of these calculations,  
100 tions, no more than a day's meteorological simulation over a small number of buildings could be run; and these extremely high-resolution simulations were not coupled with simulations incorporating feedback to the system from large-scale meteorological processes or from land surface characteristics. Reza [20] used the ENVI-met model (centimeter resolution that includes landscape characteristics)  
105 istics) to simulate microclimate impacts on an embedded realistic neighborhood morphology, but it did not include direct and diffuse radiation incident on the buildings or the terrain in the simulation and did not model large-scale effects and their impact on the microclimate. However, 2 days in 2007 and 2 days in

2017 were simulated and compared. Building energy use data were gathered for  
110 the 2 years and compared to determine that changes in morphology had affected  
the building energy use.

Thus, much has been accomplished in this area of research. But until now,  
experiments comparing the response of changes in urban form to both large-  
scale and micro-meteorological conditions for specific locations have not been  
115 conducted; and year-long simulations at building level and annual temporal  
extent have not been run.

Because it is insufficient to simulate building energy use, microclimate and  
urban energy systems in isolation [21], we integrate three different approaches  
to address these gaps: (1) numerical weather prediction (NWP) modeling at  
120 neighborhood resolution with new urban terrain inputs; (2) geographic infor-  
mation science for geospatially explicit, building-by-building urban planning and  
development; and (3) high-performance multi-building energy simulation. Our  
methodology is applied to two climatically and morphologically distinct loca-  
tions: the Oak Ridge National Laboratory (ORNL) campus in Oak Ridge, TN,  
125 and the Loop area in Chicago, IL. The Chicago location was chosen because of  
the opportunity to examine the effects of different urban morphologies for the  
proposed new Clark-Roosevelt addition southwest of the Loop (Figure 1). The  
novelty of our work is that it (1) creates new neighborhoods based on character-  
istics of an existing neighborhood, (2) examines the effects of the urban form of  
130 these new neighborhoods on weather and building energy use response at the  
resolution at which it is most relevant, and (3) accomplishes these simulations  
within a framework that allows multiscale feedbacks to and from larger-scale  
processes. This work prepares the way for similar studies using global climate  
projections as boundary conditions, along with population and urbanization  
135 estimates for future decades.



Figure 1: South side of the Chicago Loop. The Clark-Roosevelt parcel is adjacent to the east of the Chicago River. Source: Google Maps

## 2. Materials and Methods

### 2.1. Numerical Weather Prediction Simulation with High-resolution Urban Topography

Five 1-year, four-domain, nested meteorological simulations for 2015 were  
140 run using the Weather Research and Forecasting (WRF) model on the ORNL  
Titan supercomputer for two locations: one for the ORNL research campus and  
four for the Chicago Loop area. Each simulation contained urban terrain inputs  
at 10 m resolution. The four simulations run for the Chicago Loop include  
one each for (1) the Loop alone, (2) the Loop with an added Clark-Roosevelt  
145 development (southwest of the Loop) proposed at the time of this study, (3) the  
Loop with added development using more dense morphology than proposed,  
and (4) the Loop with added development using medium density but wider-  
spread morphology. The horizontal resolution for each of the domains (from  
outermost to innermost) was 6750 m, 1350 m, 270 m, and 90 m, respectively;  
150 and each used 40 vertical levels with a model top of 100 hPa as defined by  
the North American Regional Reanalysis (NARR) data set [22] used as initial

Table 1: Numbers of grid cells for nested domains of simulations

Location	d01	d02	d03	d04
Oak Ridge	100x100	85x95	80x90	96x90
Chicago	100x100	85x95	95x105	96x90

and boundary conditions. (NARR includes 29 vertical layers. Additional layers were included in this study for further examination of the processes below the urban canopy. Results of those examinations are not reported here.). Horizontal nesting is shown in Figures 2 and 3. The number of grid cells in each domain is given in Table 1.

The timestep used for the outermost (6750 m) domain was 10 seconds. The timestep for each nested grid was in the same ratio to the outer domain as was its spatial dimension. As can be inferred from the horizontal resolution, nesting ratios for these simulations are 5:1 for the outer three domains and 3:1 for the innermost domain. These ratios are based on recommendations from [23] to align U and V velocities calculated at edges of the parent-to-child Arakawa C-grids with mass quantities calculated at the centers of these cells. The simulations were run as 12 one-month simulations, each with an 18-hour spinup using original initial and boundary conditions from corresponding times from the NARR data set.

Physics packages for WRF were chosen based on optimum packages for urban scenarios and on radiation profiles. The most significant packages are shown in Table 2. New Goddard calculations of direct, direct normal, and diffuse radiation were enabled within the Registry.EM.COMMON module before compilation of the WRF code.

Table 2: Physics packages for WRF simulation

Domain	Microphysics	Radiation	Cloud Fraction	Cumulus	Surface Physics	Land	PBL	Urban Params
d01	Single Moment 3-class	New Goddard	Xu-Randall	Kain-Fritsch	Monin-Obukhov	Noah	BouLac	Urban Canopy
d02	Single Moment 3-class	New Goddard	Xu-Randall	Kain-Fritsch	Monin-Obukhov	Noah	BouLac	Urban Canopy
d03	Single Moment 3-class	New Goddard	Xu-Randall	Betts-Miller-Janjic	Monin-Obukhov	Noah	BouLac	New 10m morphs
d04	Single Moment 3-class	New Goddard	Xu-Randall	Betts-Miller-Janjic	Monin-Obukhov	Noah	BouLac	New 10m morphs

## Oak Ridge Domain Configuration

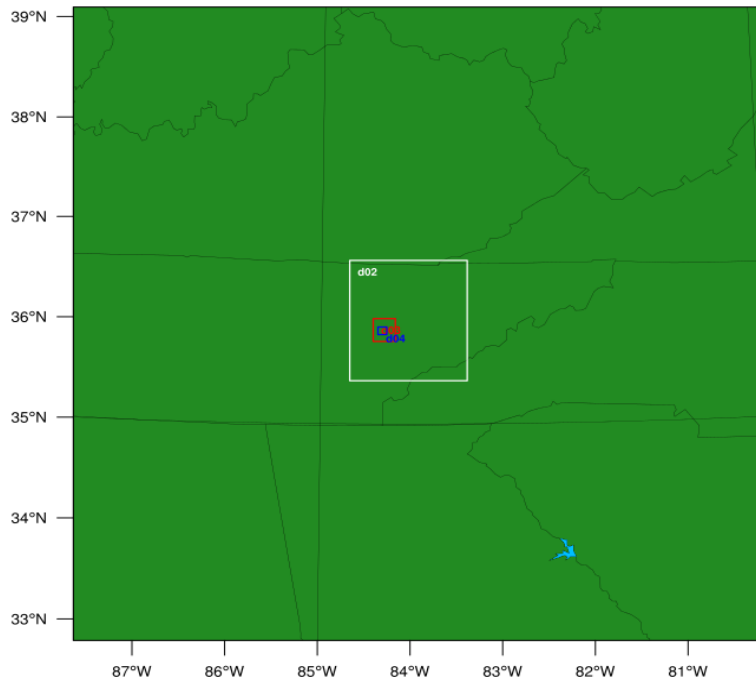


Figure 2: Nested domains for the Oak Ridge National Laboratory campus

### Chicago Domain Configuration

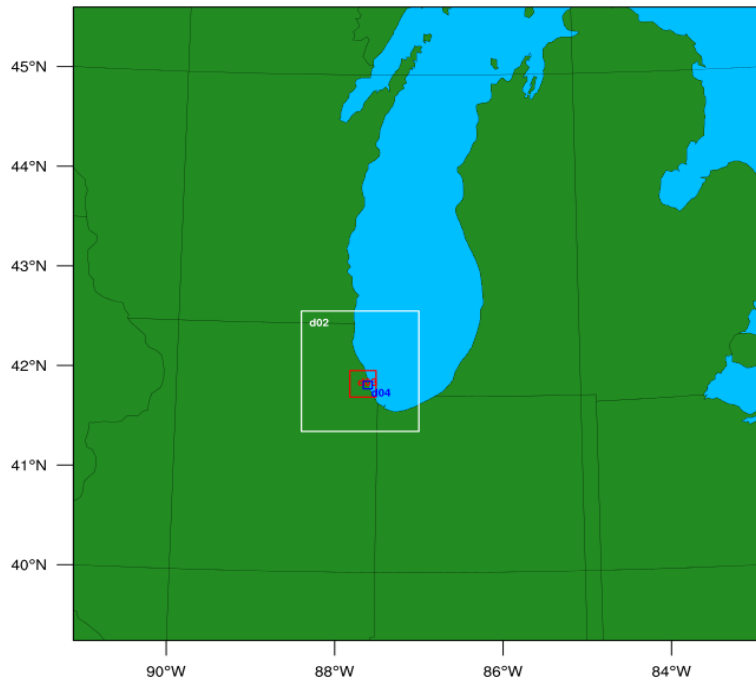


Figure 3: Nested domains for the Chicago Loop

Landcover characteristics were read into WRF from the US Geological Survey National Land Cover Database (NLCD) [24] at 30 m resolution, which provides urban land classifications such as percentage of coverage of constructed materials, percentage of impervious surface, and percentage of tree canopy cover. Urban topography at 10-m resolution was generated using LiDAR (Chicago) and in-house data (ORNL) converted to shapefiles of building footprints and corresponding building heights. Height and window-to-wall ratios for each facade of ORNL buildings were measured using a handheld, laser-based measurement tool.

The procedure to obtain the urban parameters from the 10 m resolution shapefiles for WRF input followed that of the National Urban Database and Access Portal Tool (NUDAPT) project [25], which provides urban terrain input data and 132 urban parameters for the WRF model at 1 km resolution. This procedure was coded in Python, and it produced files for each topography as data arrays in big endian format. To isolate effects of the different new neighborhoods on the Chicago Loop, the innermost domain of the WRF simulations of the Chicago Loop did not include the remainder of the city around it, although urban canopy parameters were included in the coarser-resolution domains.

The morphologies for the new development were created to test climatic response to differing densities and geometric arrangements of buildings, while holding the land parcel and adjacent morphology (i.e., the existing Chicago Loop) constant. The design for the new morphologies was approached through the concept of *urban tissues* [26], or blocks of buildings sharing a common size, shape, and material [27]. Tissues were drawn from the existing Chicago Loop. The city planners' proposed Clark-Roosevelt development was defined as mixed use: residential and commercial with the intent to encourage activity in the area. News sources indicated the sale of the land, and speculations of plans were publicized in various neighborhood/city news sources and on the developers website. To model the proposed development, Google Maps was referenced to locate buildings within the existing Loop with similar usage to those proposed in the publicized plans. These buildings were then replicated and placed in the

land parcel for the development proposed (Morph 1). Alternative high-density (Morph 2) and medium-density (Morph 3) morphology also contained buildings  
205 created from the urban tissue, with building types explicitly defined for the purposes of assessing building energy use.

## *2.2. Geographic Information Science for Geospatially Explicit, Building-by-Building Urban Planning and Development*

Post-processing of the WRF output produced weather summaries for each  
210 building in the study area, which included diagnostic variables: 2-m height temperature and 10-m height wind speed and direction, along with post-calculated relative humidity and dew point (from 2-m water vapor, 2-m temperature and surface pressure), and direct normal and diffuse longwave radiation. Geographical Information Science (GIS) procedures were used to allocate relevant WRF  
215 meteorological variables within each 90 m grid cell to the building closest to them. One weather .csv file was created for each building. The weather building ID matched the building ID in the building footprint csv/sylk file. These files were then converted to .epw format for ingestion into the U.S. Department of Energy (DOE) EnergyPlus [28] building energy simulation model. This process was completed for each of the four WRF simulations. Thus, four different  
220 sets of weather input files were provided for four separate multi-building parallel EnergyPlus simulations.

## *2.3. High-performance Multi-building Energy Simulation*

EnergyPlus was used in this study because of its performance compared  
225 against that of all other major building simulation engines as part of ANSI/ASHRAE Standard 140 [29]. This standard provides a series of test cases to ensure proper physics calculations for simple buildings. EnergyPlus has also been empirically validated using well-instrumented experimental facilities to ensure simulation results match measured data in complex buildings under input uncertainty [30].

230 In addition to uncertainty regarding simulation engine fidelity, there are legitimate concerns over the accuracy of simulation inputs as defined by a specific

building energy model. To quantify uncertainty or address validity for individual models of buildings, the International Measurement & Verification Protocol (IP-MVP) [31] or ASHRAEs Guideline 14 (G14) [32] provides a transparent process  
235 for demonstrating a models accuracy or metric-based guidance on what constitutes a good model in terms of matching measured building performance data, respectively. Both require measured data from the building being modeled.

This study shows the effect of microclimate variation on building energy for two geographical areas: (1) Oak Ridge National Laboratory using three common  
240 U.S. building types and (2) Chicago using hypothetical building morphologies that could be constructed. Since there is no measured data in either case, this study utilizes building energy models to quantify relative building energy performance as impacted by microclimate variation. The reader is cautioned against extrapolating absolute energy quantities reported in this study.

*Whole building energy analysis.* To ascertain the impact of building-level weather  
245 on annual heating and cooling loads, three representative buildings were selected for comparative simulations: a medium office building (Bldg 1: 4,982 m<sup>2</sup>), a highly efficient residential home (Bldg 2: 382 m<sup>2</sup>), and a Home Energy Rating System Building Energy Simulation Test (HERS BESTEST [33]) Case L100A  
250 building (Bldg 3: 143 m<sup>2</sup>). EnergyPlus was used to estimate energy use by these buildings informed by both measured weather data and WRF output. Energy cost per building was calculated by converting GJ values to kWh and assessing at \$0.10 per/kWh (assuming electricity was used for both heating and cooling).

*OpenStudio geometry generation.* New code written in Python to interact with  
255 the Python bindings (not standard in the official download version) for a self-compiled version of OpenStudio was used to ingest known building properties into EnergyPlus and to generate the geometry for every building described and included in an input file. Output included EnergyPlus input data files (IDFs) and OpenStudio building model (OSM) files for each building.

260 *Prototype building generation.* A modified version of the OpenStudio-Standards  
gem was used to create individual prototype buildings for each location using  
the 16 American Society of Heating, Refrigerating and Air-Conditioning Engi-  
neers (ASHRAE) Standard 90.1 [34] prototype buildings, 16 climate zones, and  
an average of 5.75 vintages (i.e., age ranges with different building codes). This  
265 modified gem has a `create_urban_met` measure that can be run in the OpenStu-  
dio graphical user interface (GUI) or from the command line using OpenStudio  
2.0. This measure must be passed the location of the geometry file generated  
from the previous code, as well as two Javascript Object Notation (JSON) files  
that define the space type mapping and heating, ventilation, and air condition-  
270 ing (HVAC) mapping, in order to support an arbitrary number of floors. This  
gem and its modification are available as open-source codes on GitHub.

*Design of experiments generation.* To quantify the most important building  
parameters (e.g., insulation level) for building energy simulation, 470 inputs  
to the building energy model were selected by subject matter experts. Inputs  
275 were those known to impact the energy use of 16 prototypical building types, 16  
climate zones, and 3 vintages that represent approximately 70% of the U.S. com-  
mercial floor space. Sensitivity analyses were then performed using an extension  
of fractional-factorial design (based on Ulrike Gromping’s FrF2 open source R  
library) that maximizes the statistical resolution for a given number of simu-  
280 lations to quantify the energy use impacts of modifications to the qualitatively  
selected building properties [35]. This process is coded with a combination of  
R and C++ and can quickly generate a full design-of-experiments permutation  
based on a single EnergyPlus model IDF, a parameters file, and a sensitivity ma-  
trix. A fully functioning command line interface allows the passing of building  
285 location to each of these files. The code then permutes the base IDF according  
to the defined parameter file and sensitivity matrix, generating newly-permuted  
variables in the IDFs. These files can then be compressed and sent to large-scale  
computing resources for simulation. This design of experiments was used to sim-  
ulate a large number of EnergyPlus runs on the ORNL Titan supercomputer

290 and to create EnergyPlus building energy models for the entire neighborhood  
in each of the five simulated morphologies for this experiment.

*ASHRAE Clear Sky Model.* Several solar models exist, of varying complexity,  
to calculate solar radiation during clear sky conditions. Among the available  
models, the ASHRAE Clear Sky Model (ACSM) is the commonly used method  
295 for estimating solar heat load for building designs. This default model, included  
in EnergyPlus, was used to estimate baseline clear-day solar radiation for each  
day of the 2015. The ACSM was initially developed for the United States or sim-  
ilarly temperate climates in the northern hemisphere. EnergyPlus calculations  
extend the clear sky application to both northern and southern hemispheres.  
300 ACSM calculates direct normal and diffuse horizontal irradiances as a function  
of extraterrestrial normal irradiance, beam pseudo optical depth, relative air  
mass, and beam air mass exponent [36]. ACSM identifies the predicted direct  
normal irradiance, on a day from each of the seasons, which should be expected  
for clear sky (and flat horizons).

#### 305 *2.4. Accounting of Model Bias Using Measurements at the ORNL Campus and at the Chicago Loop*

To identify bias in the model simulations, validation of the ORNL simula-  
tions was performed for both the 270 m and the 90 m resolution WRF output,  
using measurement data from two on-campus meteorological stations and build-  
310 ing energy performance data for two buildings. Figure 4 shows the measurement  
data available and the placement of the 90 m grid relative to the buildings on  
the ORNL campus.

The ACSM and measured data were used to identify values from the WRF-  
simulated weather files that exceeded locally observed ranges or physically real-  
315 istic solar radiation values. Comparisons of meteorological tower measurements  
(towers A, B, and D; tower A is not shown on the map in Figure 4, but its  
location is just southeast of the map extent) of temperature at 2 m above the  
ground and of surface pressure to WRF-simulated values for the domain at 90-m

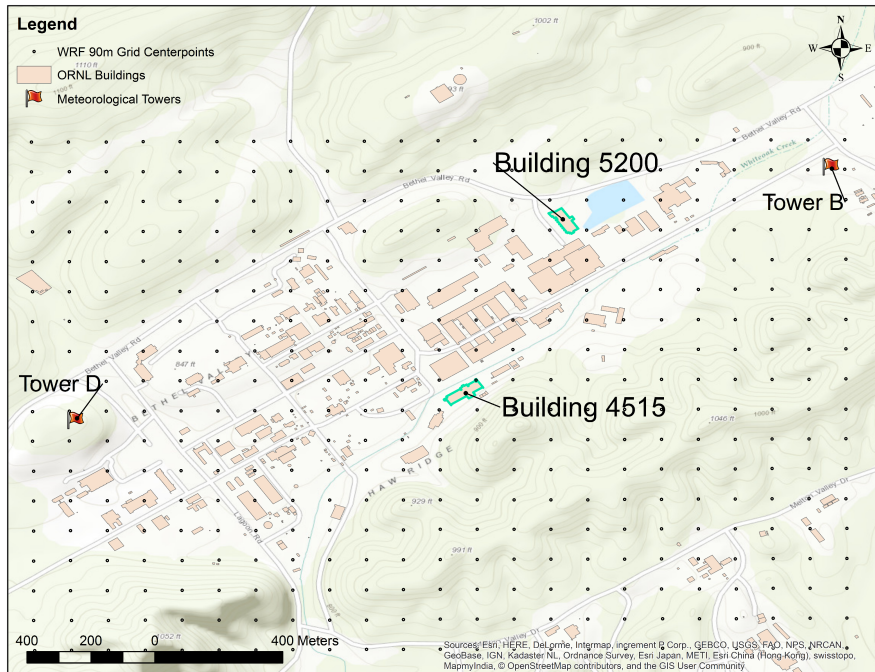


Figure 4: Sources of meteorological measurement data on the Oak Ridge National Laboratory campus. Dots represent the WRF 90m grid centerpoints, salmon colored shapes are the ORNL campus buildings, and red flags indicate the meteorological towers.

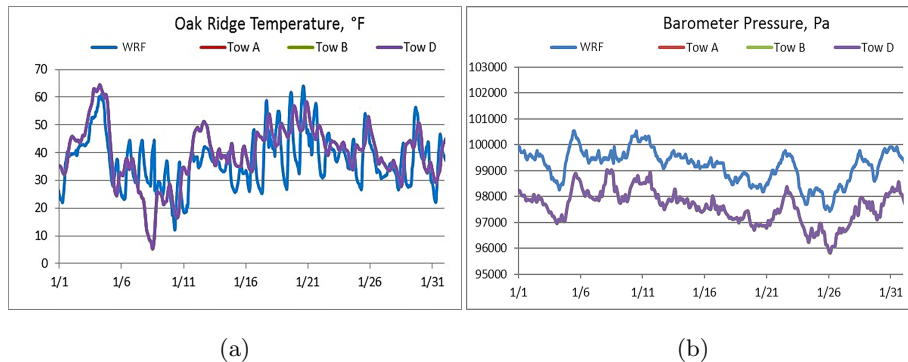


Figure 5: Comparison of WRF 90-m horizontal resolution (a) 2 m temperature (F) and (b) surface pressure (Pa) output with measured data indicated by tower at three meteorological stations. (Data from the three towers plot on top of each other showing only Tower D.)

horizontal resolution for those variables are shown in Figure 5. Simulated hourly  
 320 temperatures fall well within the bounds of the measured temperature throughout the month of January, although maxima and minima do not always occur at the same times. Pressure highs and lows track well with the measurements, although the model shows a high bias of approximately 20 hPa throughout the month.

325 Statistical comparisons of measurements of relative humidity (%) and wind speed (m/s) values and WRF output for the ORNL campus are shown in Figure 6. The WRF values are taken from the domain simulated at 270-m horizontal resolution. For each comparison, for each month of each of the data sets, hourly data is sorted into two quantiles. Those labeled “Meas” are from the measured  
 330 data. Those labeled “Set-1” are from the WRF simulation. The figure shows that WRF tends to underestimate relative humidity by approximately 10–20% and to overestimate wind speed by approximately 2–4 m/s. WRF also tends to generate much more variability in wind speed than is observed at the ORNL meteorological stations. Wind roses in Figure 7 confirm not only the greater  
 335 variability in WRF-simulated wind speeds but also the greater variability in its simulations of wind direction. The overall direction, however, is consistent with the observations.

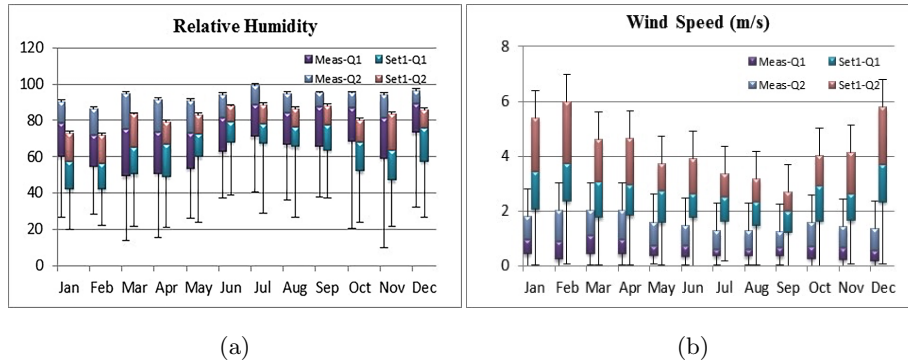


Figure 6: Comparison of WRF 270-m horizontal resolution (a) 2-m relative humidity (%) and (b) 10-m wind speed (m/s) output with measured data at three meteorological stations. Here, Meas indicates the measured data and Set1 indicates the WRF simulated data

Table 3 shows a statistical summary of measured and WRF-simulated 2015 hourly weather data for major weather variables for the ORNL campus. Model bias is evident here. Some of the bias is generally characteristic of the model [e.g. 37], and some may be due to the sensitivity of the model to urban parameters. For example, heat exchange between urban areas and the atmosphere was shown by [38] to be greatly influenced by the presence of buildings, their thermal properties, and differences in urban geometry.

Some of the difference between modeled and measured data can be attributed to the representation and parameterization of the planetary boundary layer (PBL) in the model. We used the Bougeault-Lacarrere (BouLac) scheme. The scheme’s closure type is 1.5-order local. It captures terrain-enhanced turbulence and represents relatively well the PBL in regimes of high hydrostatic equilibrium with respect to vertical displacement [39]. However, it does not account well for deep vertical mixing associated with large eddies [40]. While the appropriateness of this scheme for the subkilometer scale has not been tested, at 1 km resolution and 25-point horizontal averaging, it was shown to produce a slightly stable upper PBL [41]. A similar local closure scheme, Mellor-Yamada-Nakanishi-Niino (MYNN), was tested at subkilometer resolution and was shown also to produce a weakly stable profile at 250 m resolution [42].

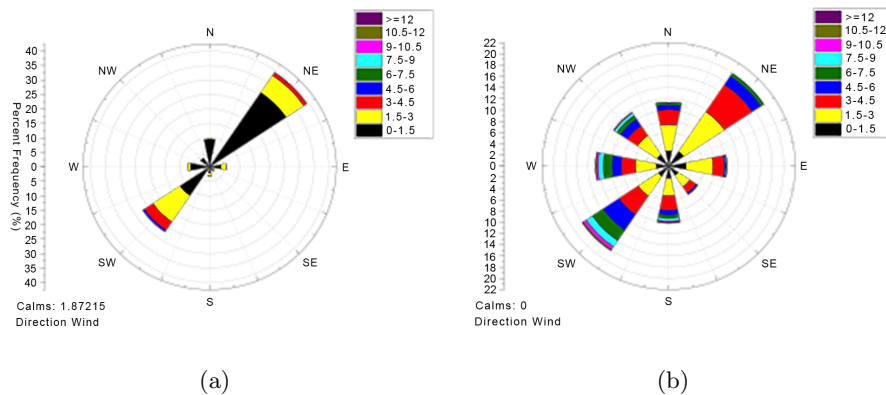


Figure 7: Comparison of wind roses generated from (a) meteorological station observations at the ORNL campus and (b) wind speeds calculated from 270-m horizontal resolution WRF output

At 1-km horizontal resolution, the BouLac scheme had a demonstrated mean bias and standard deviation for 2 m temperature of -0.32 C and 1.12 C, respectively; for relative humidity of -0.41% and 3.76%; and for 10 m wind speed of 2.5  $ms^{-1}$  and 1.07  $ms^{-1}$  [43]. The  $R^2$  values for each of these variables were 2 m temperature: 0.8 among values ranging from 0.73 to 0.8 for 8 PBL schemes; 2 m relative humidity: 0.35 among values ranging from 0.28 to 0.39; and wind speed: 0.35 among values ranging from 0.29 to 0.44. Additionally, the sensitivity of surface input parameters in the output of the WRF Single-Layer Urban Canopy Model, determined by Monte Carlo simulation by [38], indicates that 2-m temperature has domain-average biases of 1.5 to 0.8 K; the 2-m specific humidity has biases from 0.5 to 0.05 g/kg; and the 10-m wind speed and wind direction have biases from 0.2 to 1.18 m/s and 0.54 degrees, respectively.

### 3. Results and Discussion

An overall summary of the weather simulation results is given first; then a more specific analysis is given for temperature, wind speed, and relative humidity. Finally, the results of the building energy use simulation are discussed. Direct and diffuse radiation results are discussed in the appendix.

Table 3: Statistical summary of measured and simulated (270 m) hourly weather data for the ORNL campus

Variable	Stat	Meas	WRF
Temperature (C)	Mean	15.25	15.50
	Median	16.84	17.50
	Minimum	-16.88	-14.40
	Maximum	33.89	32.50
	StDev	9.51	8.44
	Kurtosis	-0.40	0.04
	Skewness	-0.49	-0.77
	$r^2$		0.79
Dew Point (C)	Mean	3.69	9.27
	Median	3.26	12.50
	Minimum	-79.99	-25.20
	Maximum	25.19	23.80
	StDev	25.22	10.21
	Kurtosis	3.21	-0.07
	Skewness	-2.09	-0.87
	$r^2$		0.53
Rel Humidity (%)	Mean	76.06	68.88
	Median	81.80	71.10
	Minimum	9.95	19.80
	Maximum	100.00	100.00
	StDev	20.20	18.33
	Kurtosis	-0.45	-0.78
	Skewness	-2.09	-0.87
	$r^2$		0.20
Wind Direction (degrees)	Mean	134.93	175.78
	Median	78.00	195.96
	Minimum	0	0.03
	Maximum	360.00	359.99
	StDev	105.68	106.50
	Kurtosis	-1.40	-1.34
	Skewness	0.36	-0.04
	$r^2$		0.04
Wind Speed (m/s)	Mean	1.09	3.24
	Median	0.76	2.78
	Minimum	0.00	0.00
	Maximum	6.64	13.76
	StDev	0.99	2.13
	Kurtosis	1.95	1.53
	Skewness	1.39	1.21
	$r^2$		0.04

### *Overall Summary of Weather Simulation Results*

375 Temperature for the Oak Ridge campus, as modeled by WRF, showed good  
agreement with meteorological station measurements, whereas pressure and rel-  
ative humidity showed slightly negative biases. Modeled wind speed for Oak  
Ridge showed a high bias of about 2 m/s; and wind direction was much more  
variable in the WRF model than in the measurements, although the dominant  
380 wind direction in the WRF output matched that measured at the meteorological  
stations. For the Chicago Loop, 3-day average hourly simulated temperature  
was biased high in the morning and in the evening but showed good agreement  
during the middle of the day for January. It was biased only low for July. Wind  
speed in the Chicago Loop was biased similarly high to that of Oak Ridge, but  
385 wind direction was even more variable with respect to that measured at the  
nearest measurement station. Simulated relative humidity in the Chicago Loop  
was biased generally high by 10–20%, and simulated pressure was consistently  
15–20 hPa low compared with observations.

### *Detailed Weather Simulation Results*

390 A single 15-minute output of 2-m height temperatures at 90-m horizontal  
resolution across the Chicago Loop is shown in Figures 8 and 9. It is represen-  
tative of an overall trend indicating that new developments to the southwest  
of the Loop are associated with cooling within the Loop. Morph 3 shows the  
largest effect, possibly indicating that the wider the horizontal area of the ad-  
dition (that is, the more massing of buildings), the more cooling. Maximum  
395 differences in temperature, water vapor, and wind speed across the Loop are  
shown in Table 4. Loop meteorology is evaluated for the area between 18th  
Street at the south end of the proposed development to the Chicago River on  
the north border of the Loop and from S. Canal Street on the west to Columbus  
400 Drive on the east. (Lateral boundaries of the WRF domain are located 16 grid  
cells to the south of the area [28th Street], 38 grid cells to the north of the area  
[Dickens Avenue], 43 grid cells to the west to Western Avenue, and 37 grid cells  
east into Lake Michigan.)

Table 4: Maximum differences across the Loop in 2-m temperature (T2) in Kelvin, 2-m water vapor (Q2) in mass fraction (kg/kg), and 10-m wind speed (WSPD10) in m/s for the Loop alone and for the Loop with each added development morphology

	T2	Q2	WSPD10
NoMorph	29	0.011	13
Morph1	31	0.011	12
Morph2	27	0.011	13
Morph3	27	0.011	10

Table 5: Morphological attributes for three potential development morphologies near the Chicago Loop

	Ftprnt Area( $m^2$ )	Height(m)	FlrSpc Area( $m^2$ )
Morph1	60,913	8,734	697,553
Morph2	115,277	41,453	3,138,167
Morph3	183,856	31,925	1,980,218

Although the differences among the morphological treatments of the Chicago Loop additions are suggestive for this single output, both 3-day (mid-month) and monthly averages of the 15-minute time steps gave a more realistic sense of the overall difference morphology made for local and extended meteorological effects. January and July averages for six variables for each morphology are presented. Of the six variables, modeled temperature showed the strongest correlation with measured data. Relative humidity was loosely correlated with measurements, wind speed was largely overestimated, and wind direction showed much more variability in the modeled results. Distinct spatial patterns were noted in monthly averages for 2-m temperature and direct and indirect irradiance in each simulation with each new added development morphology, potentially affecting the monthly and annual energy usage in each block differently.

**Temperature.** As shown in Table 3, the meteorological variable with the highest correlation to measurement data at 270-m horizontal resolution is tem-



Figure 8: Single 15-minute output of 2-m temperature variation across the Chicago Loop for the existing Loop and for the Loop with an additional new neighborhood. (a) shows the variation in temperature across the Loop without the additional development. (b) shows the Loop with the currently proposed new neighborhood (Morph 1). Figure 9 shows the Loop with each of the other two neighborhoods that were considered. Time stamp for this output is January 1, 2015, at 2:00:00 pm. Temperatures range from 34.5 to 35.5 degrees Fahrenheit. Legend is shown in Figure 9.

perature at 2-m height. Annual minima and maxima are similar, as are mean and median. The distributions skew in the same direction, but the tail thick-  
 420 ness is closer to a normal distribution in the WRF output than in the measured data. Comparisons of 3-day average hourly temperature averaged spatially over the Chicago Loop and added morphologies for each on January 9–11 and July 9–11 are shown in Figures 10 and 11. Three-day averages of hourly 2 m temperature, 2 m relative humidity, and 10 m wind speed and direction across the  
 425 Chicago Loop were calculated for both January (9–11) and July (9–11) and compared with 3-day averages of observations at the KILCHICA199 (located northwest and outside of the Loop) weather station for the same dates. For January, 8–11 a.m. temperatures simulated for the existing Loop show good



Figure 9: Single 15-minute output of 2-m temperature variation across the Chicago Loop for the existing Loop and two different additional neighborhoods. (a) shows the Loop with the high-density neighborhood (Morph 2); (b) shows the Loop with a medium-density neighborhood (Morph 3) spread farther across the parcel horizontally. Time stamp for this output is January 1, 2015, at 2:00:00 pm. Temperatures range from 34.5 to 35.5 degrees Fahrenheit.

agreement with the KILCHICA199 observations. Early morning and evening  
 430 are 1–2 degrees higher in the model results. All of the simulations with added  
 new development show temperatures from 1 to 6 degrees below the observed val-  
 ues. The simulations using three new developments plot fairly closely together  
 throughout the diurnal period, showing less than 1 degree of difference, which  
 is within the model bias. Morph 3 shows the lowest values. The waviness in  
 435 the results from the simulations including the new neighborhoods may indicate  
 atmospheric instability due to streamline deformation with the addition of new  
 buildings within the relatively low PBL height of the Chicago winter [44, 45].

July values for all simulations showed a similar curve to those of the observa-  
 tions, although the simulated values were about 10 degrees lower. The simula-  
 440 tions that included the new neighborhoods generally showed temperature about  
 3 degrees lower than the simulation with the Loop as it is currently built, and

approximately 13 degrees lower than the values measured at KILCHICA199.

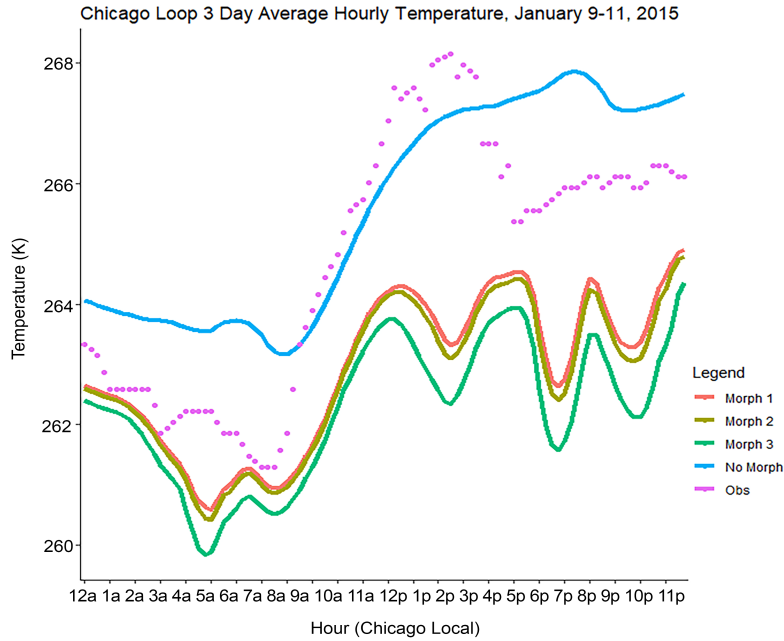


Figure 10: Comparison of 3-day hourly average 2 m temperature (K) for the Chicago Loop and Loop with added new neighborhood morphologies with 3-day hourly average observations at the KILCHICA199 weather station, January 9–11, 2015

The spatial distribution of the January average of modeled 2 m temperature at 90-m horizontal resolution is shown in Figure 12. Note a few features of the  
 445 270-m horizontal resolution domain output (not shown) in which large concentric circle temperature patterns encompassing the Chicago Loop are centered on Lake Michigan. For January, 2015, the highest 2-m temperatures over Lake Michigan are in the center of the Lake, with cooler 2-m temperature rings surrounding it. The coolest patches approach the shore, but warmer areas occur  
 450 at the land-lake interface. The Loop sits in an overall warmer ring but shows variations throughout at 90-m horizontal resolution (Figure 12), possibly due to the influence of various building heights, footprints, or functions. For the current Loop in January 2015, average temperatures are lowest (18.1–19 F) over

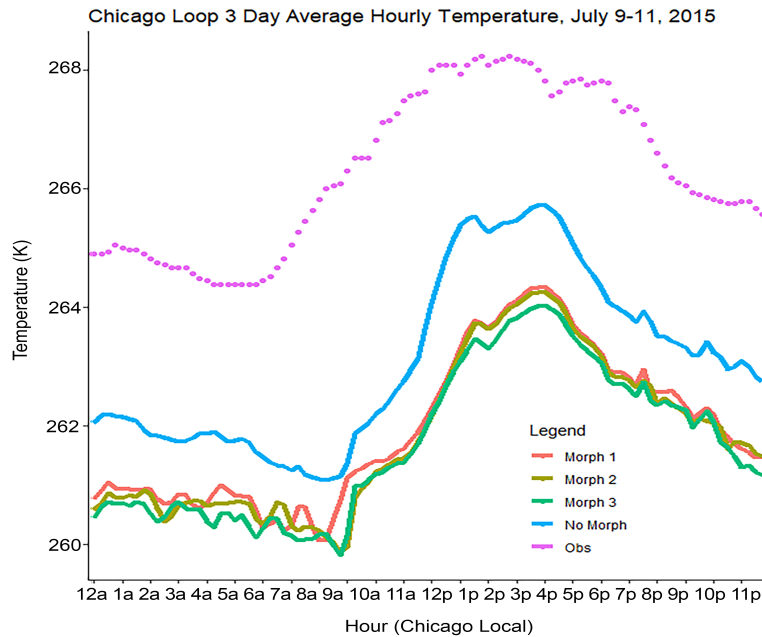
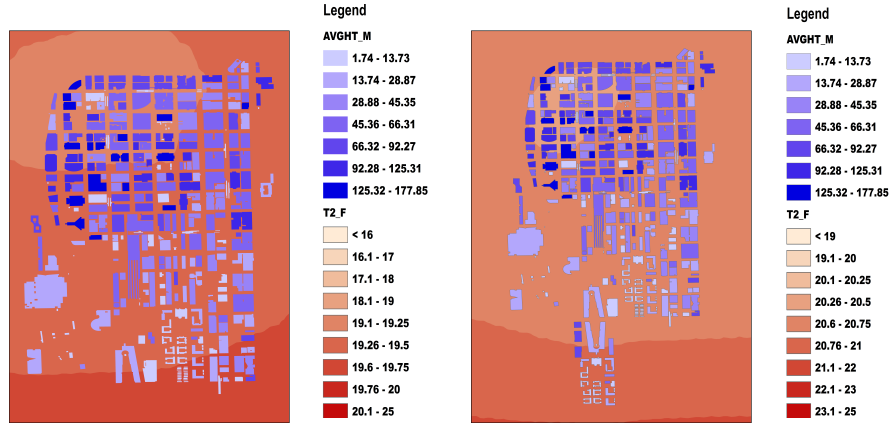


Figure 11: Comparison of 3-day hourly average 2 m temperature (K) for the Chicago Loop and Loop with added new neighborhood morphologies with 3-day hourly average observations at the KILCHICA199 weather station, July 9–11, 2015

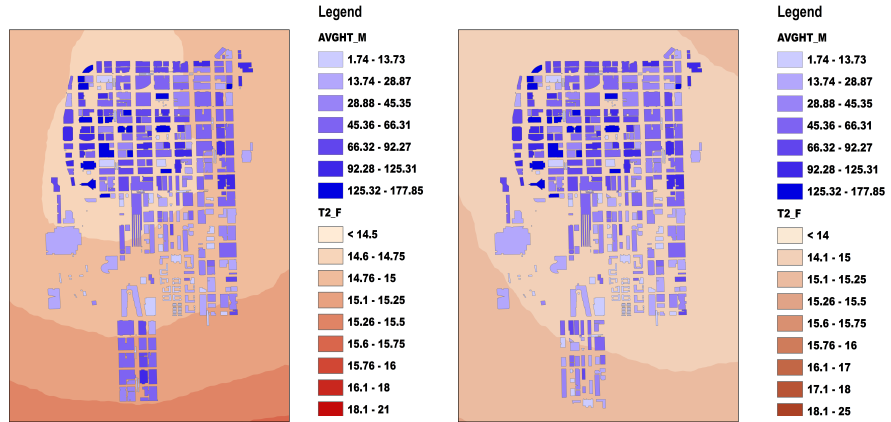
the northwest portion of the Loop and highest (19.6–19.7 5F) over the south.  
 455 The temperature of the greatest area of the Loop is, on average, 19.26–19.5 F.  
 Less variation and slightly higher temperatures are seen with the addition of  
 development Morph 1, which shows an average of 20.26–20.5 F over most of the  
 Loop, with 20.6–20.75 F in the southern portion of the area. The Loop with de-  
 velopment Morph 2 shows a cooler circular pattern with an innermost cool area  
 460 (around 14.5 F) over the northwest portion of the Loop. This is the part of the  
 Loop in which the tallest buildings stand. Concentric temperature rings around  
 that area are 14.76–15 F, 15.1–15.25 F, and 15.26–15.5 F, respectively. The  
 Loop with development Morph 3 shows a similarly cool and relatively uniform  
 low temperature ( 14 F) over the entire loop with a surrounding ring of slightly  
 465 higher temperature (14.1–15 F). Thus, we see that in January, both average

magnitude and average variation in temperature across the Loop correspond to different morphological configurations of additions to the Chicago Loop area.



(a) Chicago Loop with no new development

(b) Chicago Loop with added new development, Morph 1



(c) Chicago Loop with added new development, Morph 2

(d) Chicago Loop with added new development, Morph 3

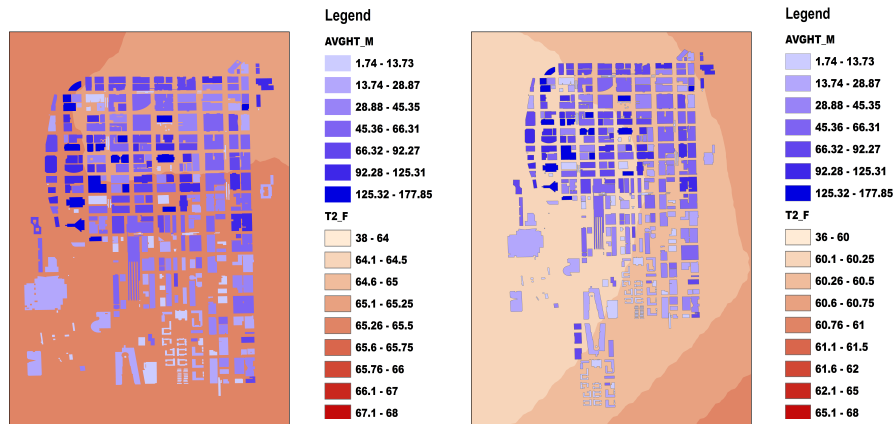
Figure 12: January average 2 m temperature in Fahrenheit. Average building height in meters is shown as blue intensity for this and similar following figures.

Results for average July 2015 temperatures across the existing Loop, compared with those across the Loop with each of the three added developments,

470 showed even greater differences in temperature among the simulations. Average July temperatures for the existing Loop were approximately 5 F warmer than for any of the three simulated with the Loop plus an additional development, and maximum and minimum temperatures were located in different areas depending on the morphology of the new development.

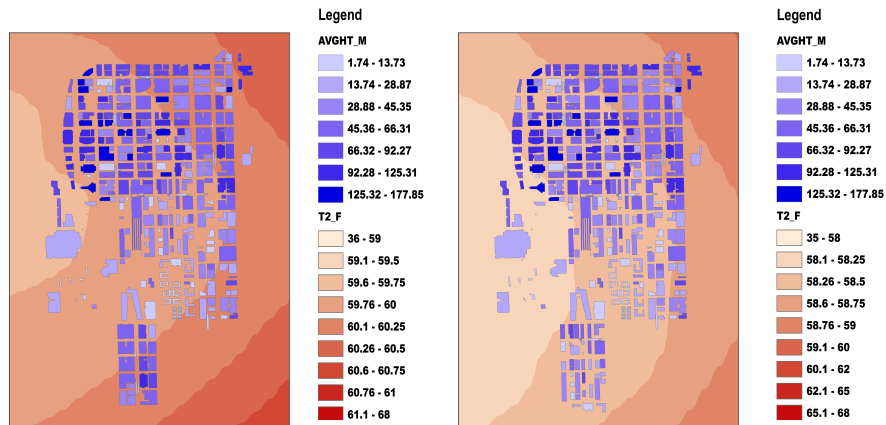
475 Spatial patterns for 2-m temperature for this domain in July were centered on Lake Michigan. The lowest temperatures over the Lake were at several centers across the Lake, each with warmer rings surrounding them. The warmest patches approached the shore, leading to an overall warmer ring in which the Chicago Loop sits (Figure 13). For each of the simulations with added new  
480 morphology, the monthly average temperature represented in the grid cells of the 90-m domain varied across the Loop in ring-like bands around a center to the west of the Loop. For the current Loop, July average temperatures were 65.1–66.25 F, with temperature over the northern portion at 64.8–65F. The bands of average temperature in the Loop with the added development of Morph 1 were  
485 around 60 F on the western side of the Loop, 60.1–60.25 on the eastern side, 60.26–60.5 further east, and 60.6–60.75z in the southeast corner of the area. The bands of average temperature in the Loop with added development of Morph 2 were somewhat cooler, beginning with 59.1–59.5 F on the western side moving to 59.6–59.75 F for the central Loop, 59.76–60 F in the northeast and southeast,  
490 60.1–60.25 F east of the area, and 60.6–60.75F in the southeast. The Loop with development Morph 3 was cooler still with temperatures around 58 F in the west, 58.1–58.25 F central, 58.26–58.5 F eastern Loop, and 58.6–58.75 F east of the area.

**Wind Speed and Direction.** As confirmed by Figures 7b and 7 and Table  
495 3, the correlation of WRF output with measured wind speed and direction is very slight. Large differences in the mean and median of both speed and direction are indicated in the table, with mean, median, and maximum wind speeds much higher in the simulated data. This result is consistent with the findings of [46]. Wind roses displayed in Figure 14 show large differences in speed, direction,  
500 and frequency between model results and measurements for simulation of wind



(a) Chicago Loop with no new development

(b) Chicago Loop with added new development, Morph 1



(c) Chicago Loop with added new development, Morph 2

(d) Chicago Loop with added new development, Morph 3

Figure 13: July average 2 m temperature in Fahrenheit.

in the current Chicago Loop.

Figure 15 shows that at 90-m horizontal resolution, average July wind patterns for the existing Loop are primarily from the southwest to the northeast. A similar pattern is shown for the Loop with the proposed new development morphology (Morph 1). In contrast, winds run west to east over the Loop for

505

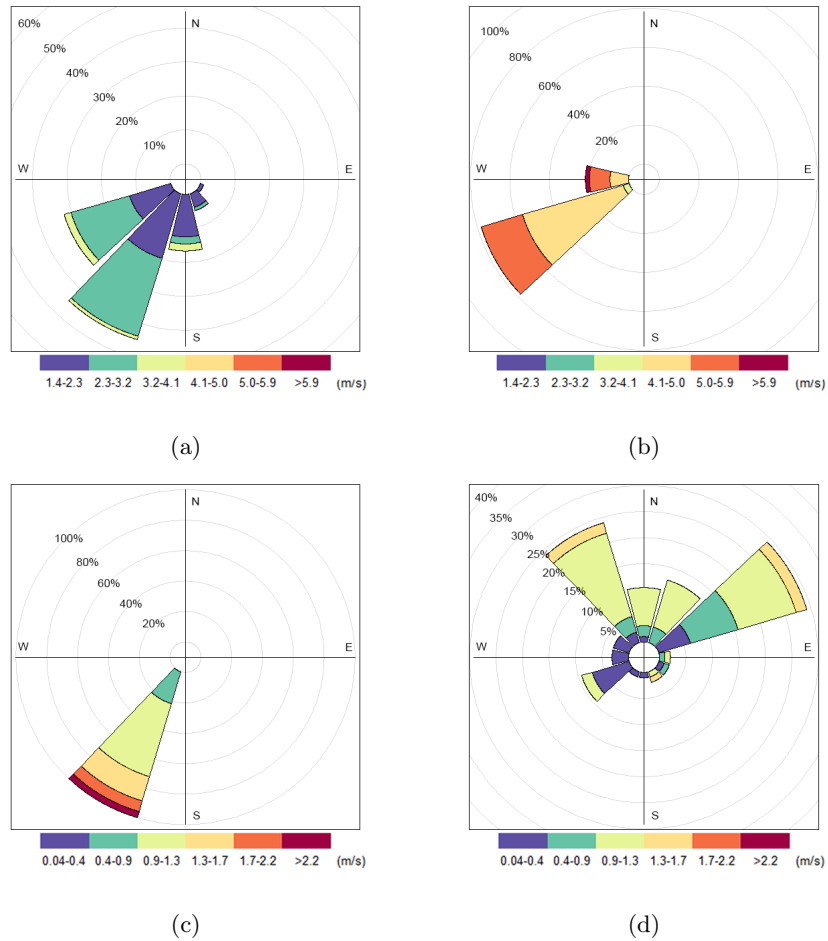
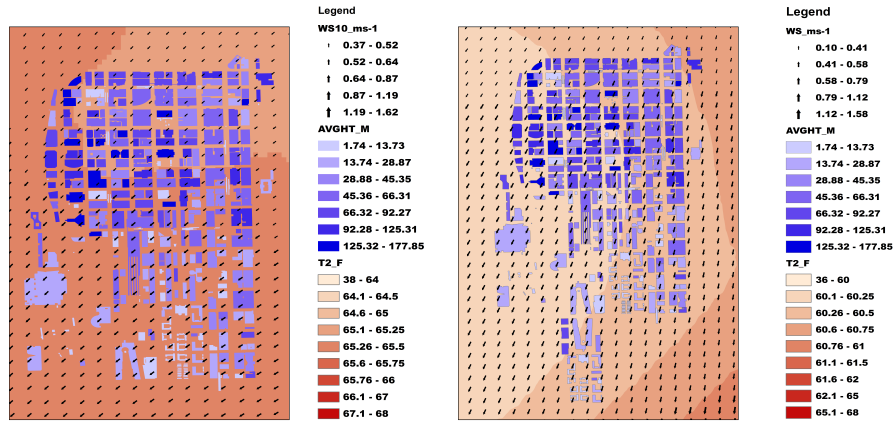


Figure 14: Comparison of 3-day average hourly 10 m wind for (a) January 9–11 observations at the KILCHICA199 weather station, (b) January 9–11 WRF output, (c) July 9–11 observations at the KILCHICA199 weather station, and (d) July 9–11 WRF output

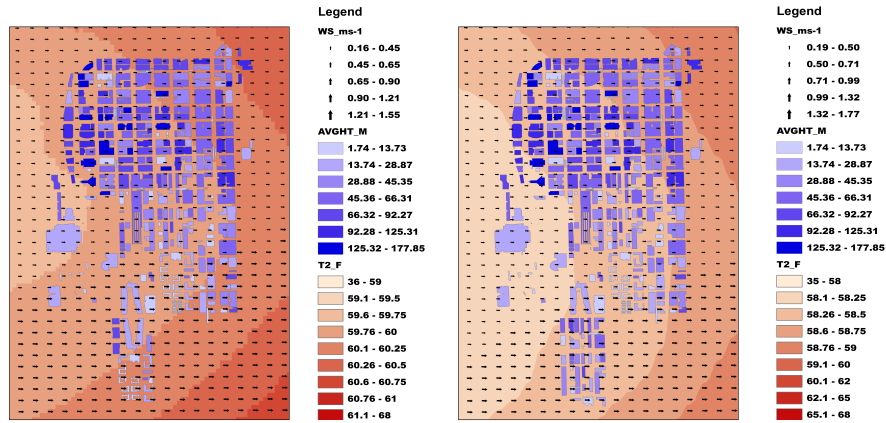
simulations with the added new high-density morphology (Morph 2) and with the added new spread-out morphology (Morph 3).

Visualization of average January 2015 wind patterns is not shown in this paper, but the most significant difference between these average wind patterns  
 510 in the original Loop and those in the simulations with the added morphologies was the overall general direction of the wind. For the original Loop, the average wind direction was south to north, whereas for the Loop with each added mor-



(a) Chicago Loop with no new development

(b) Chicago Loop with added new development, Morph 1



(c) Chicago Loop with added new development, Morph 2

(d) Chicago Loop with added new development, Morph 3

Figure 15: July average 10 m windspeed and direction

phology, the average wind direction was west to east. Changes in January wind magnitude across the Loop occurred for the Loop simulation with added development Morph 3, wherein the magnitude increased over the tallest buildings in the northern part.

**Relative Humidity.** Average monthly relative humidity values at 270 m

resolution showed some correlation with measured values. However, the mean and median for the measured values were greater than for the simulated values, and the minimum measured value was ten percent less than the simulated minimum value. Thus, the distribution of the measured values had a longer left tail than did the simulated values.

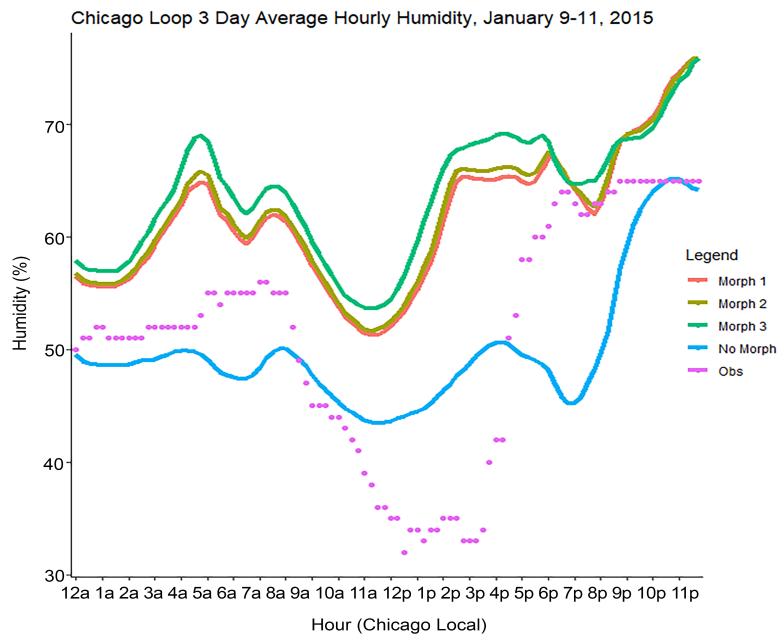


Figure 16: Comparison of 3-day hourly average 2 m relative humidity (%) for the Chicago Loop and the Loop with added new neighborhood morphologies with the 3-day hourly average observations at the KILCHICA199 weather station, January 9–11, 2015

The January and July spatially averaged 3-day average hourly relative humidity (Figures 16 and 17) failed to capture the large afternoon decrease in January but showed a more similar trend to observations in the July results. Simulation outputs incorporating the different new neighborhoods plotted fairly closely together, but they had higher values than the simulation without the new neighborhoods—by as much as 20% in the morning and evening in January and in the afternoon in July. None of the January or July simulations showed much

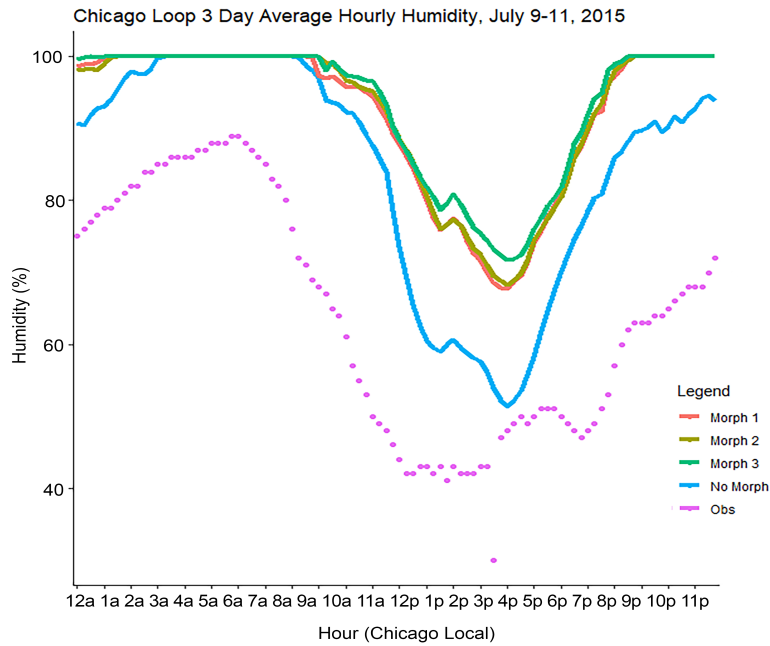


Figure 17: Comparison of 3-day hourly average 2 m relative humidity (%) for the Chicago Loop and the Loop with added new neighborhood morphologies with the 3-day hourly average observations at the KILCHICA199 weather station, July 9–11, 2015

530 spatial variation in relative humidity at 90-m resolution across the Loop (Figures not shown). Some difference in these spatially constant values was seen, however, among the different morphological configurations.

For example, average January, 2015, relative humidity values for the original Chicago Loop were between 75.1 and 77%. For the Loop with development  
 535 Morphologies 1 and 3, values were between 63 and 71%. Values for most of the Loop with development Morph 2 were 75.1–77%, but with heavier humidity in the northwestern part between 77.1 and 79%.

Average July, 2015, relative humidity values for the original Loop were between 73.1 and 75%. For the Loop with development Morph 1, values were much  
 540 higher, between 81.1 and 83%. July values for most of the Loop with development Morph 2 were 85.1–100%, with lighter humidity in the southeastern part

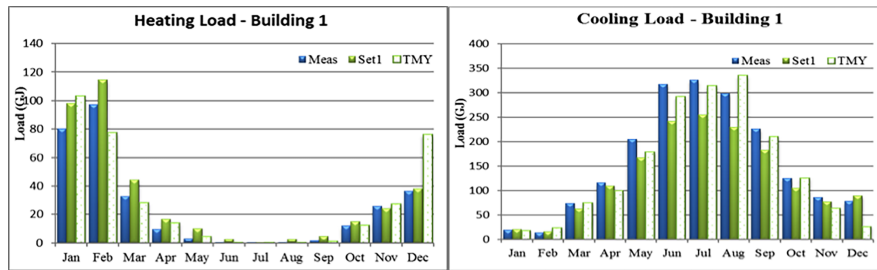
between 81.1 and 83%. The Loop with development Morph 3 showed heavier humidity diagonally across the southwest section of the loop (85.1–100%) and lighter humidity diagonally northeast (81.1 and 83%).

545 *3.1. Impact of Neighborhood Morphology on Building Energy Use*

Heating and cooling loads for three different building types in the Chicago Loop are shown in Figure 18. These loads represent side-by-side comparisons of HVAC system loads based on measured, WRF-simulated, and Typical Meteorological Year data. The presented data, charts, and statistical summaries show  
550 differences of individual meteorological weather variables and translate those differences into energy consumption values for a typical medium office building. While weather variables differ substantially, and monthly heating and cooling loads are quite different, the total annual energy consumption of the buildings using measured versus simulated weather data is similar.

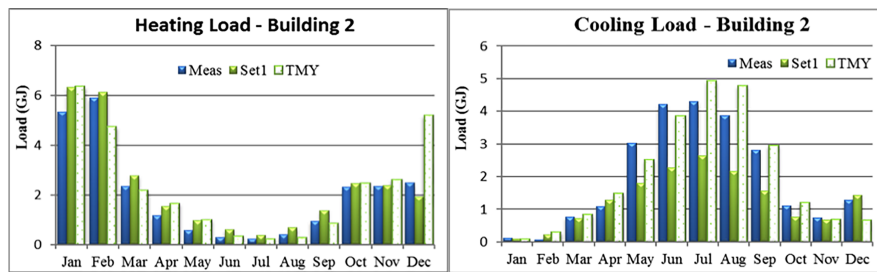
555 Figure 19 shows the energy use for buildings in the existing Chicago Loop in terms of total annual energy costs. There is no clear trend for the impact of an individual weather variable across all the building types. The dry bulb temperature, even though it is the closest match between the measured and the WRF-simulated (Set 1) data, shows the largest variance in annual energy  
560 consumption.

This figure is an effort to generalize results. A building energy model of an average medium office building ( $4,982\text{ m}^2$ ) was used to translate the differences in weather variables into differences in annual energy consumption and operating costs. The annual energy consumption of the medium office shows annual oper-  
565 ating expenses varied by up to 9.1% using the simulated, rather than the actual, meteorological station data. In an effort to determine the major contributors to this difference, the measured data was used but individual meteorological parameters were substituted using a single simulated weather parameter. Although the dry bulb temperature was relatively close to the measured data, it  
570 was the major source of difference in terms of building energy consumption, with solar radiation and wind speed contributing minor differences.



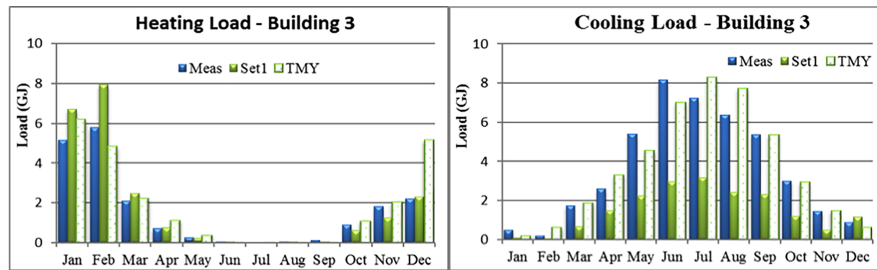
(a) Heating Load, Building 1

(b) Cooling Load, Building 1



(c) Heating Load, Building 2

(d) Cooling Load, Building 2



(e) Heating Load, Building 3

(f) Cooling Load, Building 3

Figure 18: Monthly heating and cooling loads of the buildings using three different weather data sources

Total annual energy costs for the existing Chicago Loop and for the Loop with new development following Morphologies 1 and 2 are given in Table 6. The added developments for Morphologies 1 and 2 increase total Chicago Loop energy use by 16% and 22%, respectively, owing to a greater total conditioned floor area for the Loop. However, Morph 2 constitutes the better urban plan-

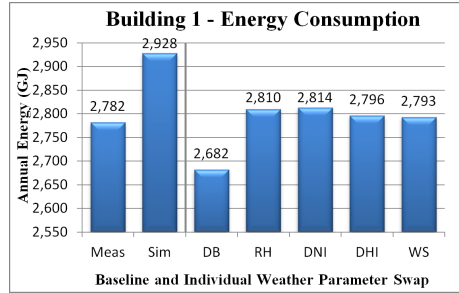


Figure 19: Dry bulb temperature (DB) is the major driving variable, shown via replacement of individual variables from the measured data (Meas) with WRF simulation data (Sim): Relative humidity (RH), direct normal irradiance (DNI), diffuse horizontal irradiance (DHI), and wind speed (WS).

Table 6: Energy consumption of buildings for three Chicago Loop morphologies.

	No. of Bldgs	Area ( $m^2$ )	Elec (GJ)	Gas (GJ)	EUI elec ( $GJ/m^2$ )	EUI gas ( $GJ/m^2$ )
No Morph	334	19,924,975	5,587,504	3,728,528	0.2804	0.1871
Morph1	361	20,892,217	6,025,625	4,754,649	0.2884	0.2276
Morph2	355	22,996,771	6,414,792	4,989,149	0.2789	0.2169

ning alternative for the Loop in terms of energy use intensity at  $0.217 GJ/m^2$  compared with Morph 1 at  $0.227 GJ/m^2$ .

#### 4. Conclusions

580 We have demonstrated a methodology for testing different morphologies for new developments in cities within a mesoscale model and have shown that the addition of even a small development to an existing neighborhood can change the microclimate of the existing neighborhood. As mesoscale models are often coupled with Earth system models to understand regional impacts of large-scale systems in the future, this methodology may be used further to understand 585 global impacts and feedbacks from changes in climate and in urban terrain due to projected changes in urban population.

With these simulations, we have observed that differences in the pattern and magnitude of climate variables across a neighborhood and among simu-

lated neighborhoods with different building morphologies can vary significantly. Because the differences in the values of ambient meteorological conditions across cities can contribute to large differences in energy usage from building to building [47], and different meteorological variables contribute differently to the overall energy usage of a building, understanding how these differences affect building energy use across a neighborhood can aid efficient neighborhood design. For example, ambient temperature contributes the most to building energy use, and direct normal irradiance contributes significantly more to building energy use than relative humidity but significantly less than temperature or wind speed [48]. Thus, the ability to generate meteorological profiles at building-level resolution, as we have demonstrated, greatly enhances the accuracy with which neighborhood energy use can be calculated. It also can suggest optimum morphological strategies, along with locations at which various energy efficiency technologies could be applied.

In this study, all initial and boundary conditions were replicated for each experiment; the only difference was in the urban terrain used. However, we recognize that urban climate simulations can be highly sensitive to model system configuration and limitations, boundary layer physics schemes, lateral boundaries [49, 50], and the quality and resolution of the input data [51, 52]. Especially given the large bias in some of the meteorological model output, specific variable values should be taken accordingly. In particular, the WRF model greatly overestimated the wind speed in this case, a variable that makes a significant difference in the persistence of nighttime urban heat islands [53]. WRF has also been shown previously [54], as well as in this study, to produce a dry bias over the central United States during summer months. Additionally, the WRF model requires large compute resources to run, and a year’s simulation at 90-m resolution takes an extremely long time to complete. Thus, generalizable information accomplished by running multiple similar experiments for different cities in different climates, although needed, would be a large undertaking possibly requiring the cooperation of many institutions. It would probably not be within the purview of a single city planner. Yet further study of the impact of urban

morphology on microclimate at resolutions of 100 m and below must be conducted to determine the full impact of building-level meteorology on building energy use. Of particular utility would be a set of experiments using different PBL schemes in conjunction with highly resolved urban terrain. Optimized  
625 boundary layer physics, or ensembles of simulations that emphasize different aspects of these processes used with this method at this resolution, could improve the results of this study. Moreover, greater certainty can be achieved as ongoing microclimate work incorporates methodological and software improvements for accurate simulation of high-resolution microclimate, via changes in  
630 mesoscale modeling, more highly resolved measurements for validation, and enhanced optimization of high-performance computing codes to run annual-scale microclimate simulations in a computationally feasible manner. Additionally, better load models—involving predictive building- and equipment-specific electrical use—are necessary to enable utility use cases including demand-side management, energy efficiency, customer education, rate structure evaluation, and  
635 compliance with emissions standards.

Nevertheless, despite these model limitations, this study adds key new methodologies for coupling microclimate modeling and building energy use, including ways of generating and testing new neighborhoods within a microclimate simulation informed by mesoscale boundaries. It also demonstrates a method for  
640 allocating building-level meteorological profiles obtained from those simulations to each building in a neighborhood-size building energy simulation. These contributions of at least comparative results represent a first step toward providing decision makers with powerful information for city growth planning that considers how regional climate may be shaped by city structure.  
645

## 5. Acknowledgments

This research was sponsored by the Laboratory Directed Research and Development Program of Oak Ridge National Laboratory, managed by UT-Battelle LLC for the U.S. Department of Energy (DOE); and by the DOE Office of

650 Science as a part of the research in Multi-Sector Dynamics within the Earth  
and Environmental System Modeling Program; and by the Exascale Comput-  
ing Project (17-SC-20-SC), a collaborative effort of the DOE Office of Science  
and the National Nuclear Security Administration. It used resources of the Oak  
Ridge Leadership Computing Facility at the Oak Ridge National Laboratory,  
655 which is supported by the DOE Office of Science.

## References

- [1] US Department of Energy, Building energy data book, [http://  
buildingsdatabook.eren.doe.gov](http://buildingsdatabook.eren.doe.gov) (2010).
- [2] S. Pincetl, P. Bunje, T. Holmes, An expanded urban metabolism method:  
660 Toward a systems approach for assessing urban energy processes and causes,  
Landscape and urban planning 107 (3) (2012) 193–202.
- [3] B. Givoni, Urban design in different climates.
- [4] V. Dorer, J. Allegrini, K. Orehounig, P. Moonen, G. Upadhyay, J. Kämpf,  
J. Carmeliet, Modelling the urban microclimate and its impact on the en-  
665 ergy demand of buildings and building clusters, Proceedings of BS 2013  
(2013) 3483–3489.
- [5] S. W. Hadley, D. J. Erickson, J. L. Hernandez, C. T. Broniak, T. Blasing,  
Responses of energy use to climate change: A climate modeling study,  
Geophysical research letters 33 (17).
- 670 [6] D. Mauree, E. Naboni, S. Coccolo, A. T. D. Perera, V. M. Nik, J.-L.  
Scartezzini, A review of assessment methods for the urban environment and  
its energy sustainability to guarantee climate adaptation of future cities,  
Renewable and Sustainable Energy Reviews 112 (2019) 733–746.
- [7] D. P. Van Vuuren, J. Edmonds, M. Kainuma, K. Riahi, A. Thomson, K. Hi-  
675 bbard, G. C. Hurtt, T. Kram, V. Krey, J.-F. Lamarque, et al., The repre-

sentative concentration pathways: an overview, *Climatic change* 109 (1-2) (2011) 5.

- [8] W. Collins, A. Craig, J. Truesdale, A. Di Vittorio, A. Jones, B. Bond-Lamberty, K. Calvin, J. Edmonds, S. Kim, A. Thomson, et al., The integrated earth system model (iesm): formulation and functionality, *Geosci Model Dev Discuss* 8 (1) (2015) 381–427.
- [9] F. Creutzig, G. Baiocchi, R. Bierkandt, P.-P. Pichler, K. C. Seto, Global typology of urban energy use and potentials for an urbanization mitigation wedge, *Proceedings of the National Academy of Sciences* 112 (20) (2015) 6283–6288.
- [10] US Energy Information Administration, Energy-related carbon dioxide emissions by state, 2000-2015, <https://www.eia.gov/environment/emissions/state/analysis/> (2018).
- [11] City of Chicago, Energy usage 2010, <https://data.cityofchicago.org/Environment-Sustainable-Development/Energy-Usage-2010/8yq3-m6wp> (2018).
- [12] California Energy Commission, Energy assessments, <https://www.energy.ca.gov/assessments> (2018).
- [13] Z. Zamani, S. Heidari, P. Hanachi, Reviewing the thermal and microclimatic function of courtyards, *Renewable and Sustainable Energy Reviews* 93 (2018) 580–595.
- [14] P. Rode, C. Keim, G. Robazza, P. Viejo, J. Schofield, Cities and energy: urban morphology and residential heat-energy demand, *Environment and Planning B: Planning and Design* 41 (1) (2014) 138–162.
- [15] H. Taha, R. Levinson, A. Mohegh, H. Gilbert, G. Ban-Weiss, S. Chen, Air-temperature response to neighborhood-scale variations in albedo and canopy cover in the real world: Fine-resolution meteorological modeling

and mobile temperature observations in the los angeles climate archipelago, *Climate* 6 (2) (2018) 53.

- 705 [16] Y. Toparlar, B. Blocken, B. Maiheu, G. Van Heijst, A review on the cfd analysis of urban microclimate, *Renewable and Sustainable Energy Reviews* 80 (2017) 1613–1640.
- [17] J. A. Dirks, W. J. Gorrissen, J. H. Hathaway, D. C. Skorski, M. J. Scott, T. C. Pulsipher, M. Huang, Y. Liu, J. S. Rice, Impacts of climate change on energy consumption and peak demand in buildings: A detailed regional approach, *Energy* 79 (2015) 20–32.
- 710 [18] X. Yang, L. Zhao, M. Bruse, Q. Meng, An integrated simulation method for building energy performance assessment in urban environments, *Energy and buildings* 54 (2012) 243–251.
- [19] R. Zhang, P. A. Mirzaei, B. Jones, Development of a dynamic external cfd and bes coupling framework for application of urban neighbourhoods energy modelling, *Building and Environment* 146 (2018) 37–49.
- 715 [20] H. M. Reza, Study on changes in micro-climatic parameters and domestic energy consumption influenced by changes in urban morphology in hatir-jheel area, dhaka.
- 720 [21] J. Allegrini, K. Orehounig, G. Mavromatidis, F. Ruesch, V. Dorer, R. Evins, A review of modelling approaches and tools for the simulation of district-scale energy systems, *Renewable and Sustainable Energy Reviews* 52 (2015) 1391–1404.
- [22] F. Mesinger, G. DiMego, E. Kalnay, K. Mitchell, P. C. Shafran, W. Ebisuzaki, D. Jović, J. Woollen, E. Rogers, E. H. Berbery, et al., North american regional reanalysis, *Bulletin of the American Meteorological Society* 87 (3) (2006) 343–360.
- 725 [23] W. Werner, Kelly Wang, Nesting in wrf, [https://www.climate-science.org.au/sites/default/files/werner\\_nesting.pdf](https://www.climate-science.org.au/sites/default/files/werner_nesting.pdf) (2017).
- 730

- [24] C. H. Homer, J. A. Fry, C. A. Barnes, The national land cover database, US Geological Survey Fact Sheet 3020 (4) (2012) 1–4.
- [25] J. Ching, M. Brown, S. Burian, F. Chen, R. Cionco, A. Hanna, T. Hultgren, T. McPherson, D. J. Sailor, H. Taha, et al., National urban database and access portal tool, nudapt.  
735
- [26] V. Oliveira, Urban morphology: an introduction to the study of the physical form of cities, Springer, 2016.
- [27] K. Kropf, Urban tissue and the character of towns, Urban Design International 1 (3) (1996) 247–263.
- [28] D. B. Crawley, L. K. Lawrie, F. C. Winkelmann, W. F. Buhl, Y. J. Huang, C. O. Pedersen, R. K. Strand, R. J. Liesen, D. E. Fisher, M. J. Witte, et al., Energyplus: creating a new-generation building energy simulation program, Energy and buildings 33 (4) (2001) 319–331.  
740
- [29] A. S. Committee, Standard 140-2017 – standard method of test for the evaluation of building energy analysis computer programs (2017).  
745
- [30] R. M. P. I. Li, Qi, J. Joe, Empirical validation of multi-zone building and hvac system models under uncertainty, in: ASHRAE/IBPSA-USA 2020 Building Performance Analysis Conference SimBuild (BPACS), 2020.
- [31] E. V. Organization, International performance measurement verification protocol - concepts and options for determining energy and water savings, EVO.  
750
- [32] A. G. ASHRAE, 14: Measurement of energy and demand savings, ASHRAE.
- [33] R. Judkoff, J. Neymark, Home energy rating system building energy simulation test (hers bestest): Volume 1, tier 1 and tier 2 tests user’s manual, Tech. rep., National Renewable Energy Lab., Golden, CO (US) (1995).  
755

- [34] US Department of Energy, 90.1 prototype building models, <https://www.energycodes.gov/901-prototype-building-models-complete-package> (2013).
- 760 [35] G. Ostrouchov, J. New, J. Sanyal, P. Patel, Uncertainty analysis of a heavily instrumented building at different scales of simulation.
- [36] A. S. Committee, et al., Ashrae handbook: fundamentals 2013 (2013).
- [37] L. Pan, Y. Liu, J. Knievel, L. Delle Monache, G. Roux, Evaluations of wrf sensitivities in surface simulations with an ensemble prediction system, Atmosphere 9 (3) (2018) 106.
- 765 [38] Z.-H. Wang, E. Bou-Zeid, S. K. Au, J. A. Smith, Analyzing the sensitivity of wrfs single-layer urban canopy model to parameter uncertainty using advanced monte carlo simulation, Journal of Applied Meteorology and Climatology 50 (9) (2011) 1795–1814.
- 770 [39] H. H. Shin, S.-Y. Hong, Intercomparison of planetary boundary-layer parametrizations in the wrf model for a single day from cases-99, Boundary-Layer Meteorology 139 (2) (2011) 261–281.
- [40] A. E. Cohen, S. M. Cavallo, M. C. Coniglio, H. E. Brooks, A review of planetary boundary layer parameterization schemes and their sensitivity in simulating southeastern us cold season severe weather environments, Weather and forecasting 30 (3) (2015) 591–612.
- 775 [41] M. A. LeMone, M. Tewari, F. Chen, J. Dudhia, Objectively determined fair-weather cbl depths in the arw-wrf model and their comparison to cases-97 observations, Monthly Weather Review 141 (1) (2013) 30–54.
- 780 [42] H. H. Shin, J. Dudhia, Evaluation of pbl parameterizations in wrf at sub-kilometer grid spacings: Turbulence statistics in the dry convective boundary layer, Monthly Weather Review 144 (3) (2016) 1161–1177.

- [43] R. F. Banks, J. Tiana-Alsina, J. M. Baldasano, F. Rocadenbosch, A. Pappayannis, S. Solomos, C. G. Tzanis, Sensitivity of boundary-layer variables to pbl schemes in the wrf model based on surface meteorological observations, lidar, and radiosondes during the hygra-cd campaign, *Atmospheric Research* 176 (2016) 185–201.
- [44] C. J. Nappo, Sporadic breakdowns of stability in the pbl over simple and complex terrain, *Boundary-Layer Meteorology* 54 (1-2) (1991) 69–87.
- [45] Y. Zhang, D. J. Seidel, S. Zhang, Trends in planetary boundary layer height over europe, *Journal of Climate* 26 (24) (2013) 10071–10076.
- [46] M. Barlage, S. Miao, F. Chen, Impact of physics parameterizations on high-resolution weather prediction over two chinese megacities, *Journal of Geophysical Research: Atmospheres* 121 (9) (2016) 4487–4498.
- [47] M. Bhandari, S. Shrestha, J. New, Evaluation of weather datasets for building energy simulation, *Energy and Buildings* 49 (2012) 109–118.
- [48] S. Pallin, P. Boudereaux, M. Stockdale, E. Beuchler, Effects of air leakage on buildings’ overall thermal resistances based on us climate zones, *ASHRAE Transactions* 123 (2) (2017) 90–101.
- [49] T. T. Warner, R. A. Peterson, R. E. Treadon, A tutorial on lateral boundary conditions as a basic and potentially serious limitation to regional numerical weather prediction, *Bulletin of the American Meteorological Society* 78 (11) (1997) 2599–2618.
- [50] R. D. Torn, G. J. Hakim, C. Snyder, Boundary conditions for limited-area ensemble kalman filters, *Monthly weather review* 134 (9) (2006) 2490–2502.
- [51] T. T. Warner, Quality assurance in atmospheric modeling, *Bulletin of the American Meteorological Society* 92 (12) (2011) 1601–1610.
- [52] S. Adam, V. Wulfmeyer, Optimizing wrf for realistic large eddy simulations, in: *EGU General Assembly Conference Abstracts*, Vol. 20, 2018, p. 14555.

- 810 [53] A. C. Varquez, M. Kanda, Global urban climatology: a meta-analysis of  
air temperature trends (1960–2009), *npj Climate and Atmospheric Science*  
1 (1) (2018) 32.
- [54] Y. Lin, W. Dong, M. Zhang, Y. Xie, W. Xue, J. Huang, Y. Luo, Causes of  
model dry and warm bias over central us and impact on climate projections,  
815 *Nature communications* 8 (1) (2017) 881.

## Appendix A. Radiation Results

Because this study focuses mostly on urban terrain, no optimized cloud-resolving parameterizations were used, although a simple cloud component was included in the simulation. Cloud cover affects direct and diffuse radiation received on buildings and ground, and temperature sensed within buildings;  
820 thus building energy use values calculated using these inputs will be affected by lack of inclusion of full cloud processes. Nevertheless, we report the simulation results for both direct and diffuse radiation.

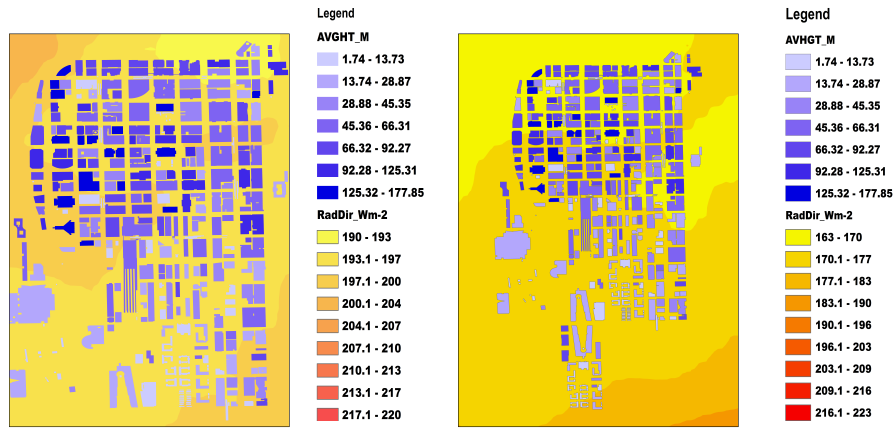
**Direct Normal Radiation.** Averaged direct normal radiation simulations  
825 for the current Chicago Loop and for the Loop with each added development morphology are shown for July in Figure Appendix A.1. Monthly values for July vary spatially across the Loop. For most of the current Loop, values range between 190 and 193  $W/m^2$ , with northwest and southeast patches receiving 197.1–200  $W/m^2$  and a northwestern patch receiving 200.1–204  $W/m^2$ . The  
830 Loop with added proposed morphology (Morph 1) shows values of 163–170  $W/m^2$  for the northwestern part of the Loop and a patch to the east. The remainder of the Loop receives 170.1–177  $W/m^2$  of direct normal irradiance. Southeast of the Loop shows values between 177.1 and 190  $W/m^2$ . The Loop with added high-density (taller, closely packed buildings) morphology (Morph  
835 2) shows a similar spatial pattern to Morph 1 but with slightly lower overall values. The Loop with added development Morph 2 shows 161–169  $W/m^2$  direct radiation for the northwestern part of the Loop and a patch of similar value to the east. The remainder of the Loop receives 169.1–176  $W/m^2$ . Southeast of the Loop shows values between 176.1 and 183  $W/m^2$ . Finally, the Loop  
840 with added lower density (shorter buildings) but wider area shows most of the Loop receiving between 172.1 and 178  $W/m^2$  direct normal irradiance, except in a few northwest spots where it receives 166–172  $W/m^2$ . Stripes to the east and southeast show direct normal irradiance at 178.1–184  $W/m^2$  and 184.1–190  $W/m^2$ , respectively.

845 For the month of January, because the sun angle is lower for the Chicago

area, direct normal irradiance is lower overall than for July (Figure not shown). Simulated values for the greater part of the current Loop in January are between 60.1 and 60.5  $W/m^2$ . A small northeastern portion receives a bit more direct normal irradiance at 60.6–61  $W/m^2$ , while a large southern portion of the Loop receives 59.1–59.5  $W/m^2$ . For the Loop with added proposed morphology (Morph 1), the northeastern tip of the Loop receives 64.6–65  $W/m^2$  direct normal irradiance, a diagonal strip just south of it running from northwest to southeast receives 64.1–64.5  $W/m^2$ , and the remainder receives 63.6–64  $W/m^2$ . A patch southeast of the Loop receives 64.1–64.5  $W/m^2$ . The Loop with added high-density (taller, closely packed buildings) morphology (Morph 2) shows average January direct normal irradiance of 60.1–61  $W/m^2$  over most of the Loop with exterior patches at 61.1–62  $W/m^2$ . Finally, the Loop with added lower density (shorter buildings) but wider area showed a circular striated pattern of diffuse radiation progressing west to east from 57.6–58 to 58.1–58.5, to 58.6–59  $W/m^2$ .

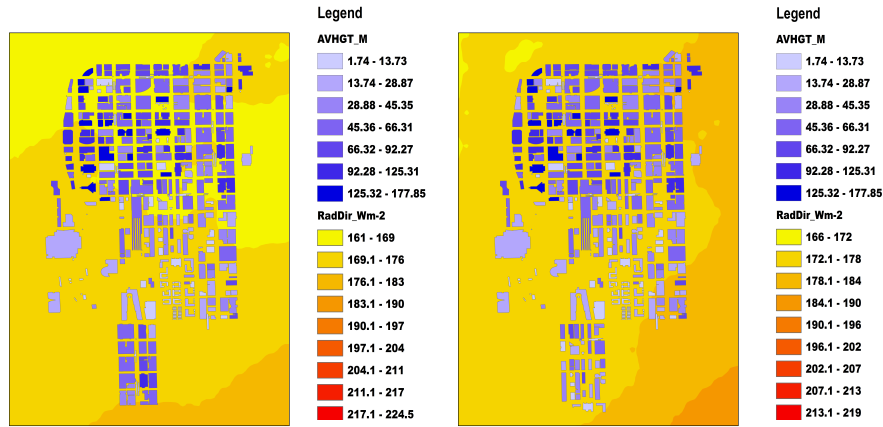
**Diffuse Radiation.** The current Chicago Loop shows average diffuse radiation for January, 2015, for the southern portion at 28.26–28.5  $W/m^2$ . For the northern portion and the extreme southeastern portion, the diffuse radiation is 28.1–28.25  $W/m^2$ . The Loop with added proposed morphology (Morph 1) shows a very different pattern of monthly average diffuse radiation. The northeastern tip of the Loop receives 24.6–25  $W/m^2$  diffuse radiation, while the southwestern side receives 26.1–26.5  $W/m^2$ . Diagonally through the center of the Loop, diffuse radiation is in the range of 25.1–25.5  $W/m^2$ . The Loop with added high-density (taller, closely packed buildings) morphology (Morph 2) shows average January diffuse radiation of 28.1–29  $W/m^2$  over most of the Loop with exterior patches at 27.1–27.5  $W/m^2$ . Finally, the Loop with added lower density (shorter buildings) but wider area shows a diagonally striated pattern of diffuse radiation progressing from 21.6 to 23.5  $W/m^2$  in 0.5  $W/m^2$  increments.

Average diffuse irradiance for the month of July Appendix A.2 is higher overall and shows a more spatially varied pattern than the month of January. The current Chicago Loop shows average diffuse radiation for July, 2015, mostly at



(a) Chicago Loop with no new development

(b) Chicago Loop with added new development, Morph 1

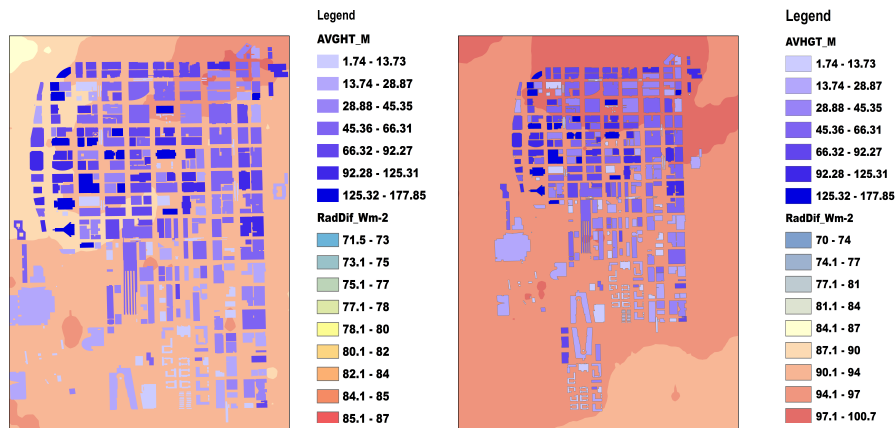


(c) Chicago Loop with added new development, Morph 2

(d) Chicago Loop with added new development, Morph 3

Figure Appendix A.1: July average direct normal irradiance ( $W/m^2$ )

82.1–84  $W/m^2$  with northeast and southwest specks of 84.1–85 and progressively western bands of 80.1–82  $W/m^2$  and 78.1–80  $W/m^2$ . The Loop with added proposed morphology (Morph 1) shows a very different pattern of monthly average diffuse radiation compared with the original Loop. The northern part of the Loop receives 97.1–100.7  $W/m^2$  diffuse radiation, while the remainder of the



(a) Chicago Loop with no new development

(b) Chicago Loop with added new development, Morph 1

(c) Chicago Loop with added new development, Morph 2

(d) Chicago Loop with added new development, Morph 3

Figure Appendix A.2: July average diffuse irradiance ( $W/m^2$ )

Loop receives 94.1–97  $W/m^2$ . Diffuse radiation of 90.1–94  $W/m^2$  reaches the area just southeast of the Loop. The Loop with added high-density (taller, closely packed buildings) morphology (Morph 2) shows average July diffuse radiation of 94.1–97  $W/m^2$  over most of the Loop with exterior patches at 97.1–100.9 and 90.1–94  $W/m^2$  (southeast). Finally, the Loop with added lower

density (shorter buildings) but wider area shows a swirled pattern of diffuse radiation with most of the area between 90.1 and 94  $W/m^2$ , except for a northwest and north central portion at 94.1–97  $W/m^2$  and thin slices in the west and  
890 southeast at 87.1–90  $W/m^2$ .